

Biophysical Journal, Volume 99

Supporting Material

Title: Modeling the Self-Organization Property of Keratin Intermediate Filaments

Authors: Jin Seob Kim, Chang-Hun Lee, and Pierre A Coulombe

# Modeling the Self-Organization Property of Keratin Intermediate Filaments: Supporting Material

Jin Seob Kim<sup>1</sup>, Chang-Hun Lee<sup>1</sup>, and Pierre A. Coulombe<sup>1,2,3</sup>

<sup>1</sup>Dept. of Biochemistry and Molecular Biology, Bloomberg School of Public Health, the Johns Hopkins University, Baltimore, MD 21205, USA  
Dept. of <sup>2</sup>Biological Chemistry, and <sup>3</sup>Dermatology, School of Medicine, the Johns Hopkins University, Baltimore, MD 21205, USA

## Contents:

- Supporting Methods
  1. Brownian Dynamics of a Rigid Rod
  2. How to Obtain the Stiffness of Tail Domain Binding
  3. Details on the Dissociation Rate Constant
  4. Computational Details
- Supporting Data
  - Supplemental Figure Legends
  - Supplemental Figures
    1. Figure S1: Simulation results without tail domain binding events
    2. Figure S2: Simulation results with tail domains as free particles
  - Supplemental Movies
    1. Movie S1: Filament network topology achieved when only tail domain binding events are included (see Fig. 1*B* in main text).
    2. Movie S2: Filament network topology achieved when tail domain binding events and long-range interactions between filaments are included (see Fig. 2*B* in main text).
    3. Movie S3: Filament network topology achieved when tail domain binding events are reversible ( $k_{\text{on}} = 5 \mu\text{M}^{-1}\text{s}^{-1}$ ;  $k_{\text{off}} = 10 \text{s}^{-1}$ ) (see Fig. 3*A* in main text).
    4. Movie S4: Filament network topology achieved when filaments are longer ( $L = 2 \mu\text{m}$ ) (see Fig. 3*B* in main text).
    5. Movie S5: Filament network topology achieved when filaments are shorter ( $L = 0.5 \mu\text{m}$ ) (see Fig. 4*C* in main text).

# Modeling the Self-Organization Property of Keratin Intermediate Filaments: Supporting Methods

Jin Seob Kim<sup>1</sup>, Chang-Hun Lee<sup>1</sup>, and Pierre A. Coulombe<sup>1,2,3</sup>

<sup>1</sup>Dept. of Biochemistry and Molecular Biology, Bloomberg School of Public Health, the Johns Hopkins University, Baltimore, MD 21205, USA  
 Dept. of <sup>2</sup>Biological Chemistry, and <sup>3</sup>Dermatology, School of Medicine, the Johns Hopkins University, Baltimore, MD 21205, USA

## 1 Brownian Dynamics of a Rigid Rod

Let us discuss the method to describe the evolution of filament network formation in detail. In this study, we apply Brownian Dynamics (BD) simulation method for rigid bodies. We also employ the Lie-group-theoretic method to describe the configurations of a rigid rod. In particular, we utilize the Special Euclidean group SE(3) for the position and the orientation of a rod. See (1, 2) for detailed explanation on the Lie-group-theoretic method. Let  $g = (\mathbf{r}, R) \in \text{SE}(3)$  denote the position and orientation of a filament. The equation of motion for a rigid rod, or so-called Langevin equation, is written as

$$\Gamma \boldsymbol{\xi} = \mathbf{F} + \mathbf{F}_R(t) \quad (1)$$

where  $\Gamma = \text{diag}(\Gamma_r, \Gamma_t)$  denotes the damping coefficient matrix. Each diagonal block element is defined as (3):

$$\Gamma_t = \begin{pmatrix} \zeta_{\parallel} & 0 & 0 \\ 0 & \zeta_{\perp} & 0 \\ 0 & 0 & \zeta_{\perp} \end{pmatrix} \quad (2)$$

with

$$\begin{aligned} \zeta_{\parallel} &= \frac{2\pi\eta L}{\ln(L/d_{\text{fil}}) - 0.2} \\ \zeta_{\perp} &= \frac{4\pi\eta L}{\ln(L/d_{\text{fil}}) + 0.84} \end{aligned} \quad (3)$$

and

$$\Gamma_r = \begin{pmatrix} \zeta_a & 0 & 0 \\ 0 & \zeta_r & 0 \\ 0 & 0 & \zeta_r \end{pmatrix} \quad (4)$$

with

$$\begin{aligned} \zeta_a &= \pi\eta d_{\text{fil}}^2 L \\ \zeta_r &= \frac{\frac{1}{3}\pi\eta L^3}{\ln(L/d_{\text{fil}}) - 0.66}. \end{aligned} \quad (5)$$

Here  $L$ ,  $d_{\text{fil}}$ , and  $\eta$  denote the length and diameter of a rod, and the viscosity of water, respectively.  $\boldsymbol{\xi} = [\boldsymbol{\omega}^T \ \mathbf{v}^T]^T$  denotes the so-called body-fixed velocity of the filament with  $\boldsymbol{\omega}$  and  $\mathbf{v}$  denoting the angular and linear velocity, respectively.  $\mathbf{F} = [\boldsymbol{\tau}^T \ \mathbf{f}^T]^T$  denotes the wrench (torque  $\boldsymbol{\tau}$  and force  $\mathbf{f}$ ) on the rigid body. This wrench includes the force and torque from the tail domain binding and/or filament-filament interactions.  $\mathbf{F}$  represents a wrench vector viewed from the frame that is rigidly attached to the rigid rod, known as the body fixed frame. So is the random excitation term  $\mathbf{F}_R(t)$ . When it represents a spatial quantity viewed from the spatially fixed or lab frame, a superscript ‘s’ is attached, as in  $\mathbf{F}^s$ . We keep this notation hereafter. By using the following matrix differential equation

$$g^{-1} \frac{dg}{dt} = \widehat{\boldsymbol{\xi}} \quad (6)$$

where

$$\widehat{\boldsymbol{\xi}} = \begin{pmatrix} \widehat{\boldsymbol{\omega}} & \mathbf{v} \\ \mathbf{0}^T & 0 \end{pmatrix} \quad (7)$$

and, with  $\boldsymbol{\omega} = [\omega_1, \omega_2, \omega_3]^T \in \mathbb{R}^3$ ,

$$\widehat{\boldsymbol{\omega}} = \begin{pmatrix} 0 & -\omega_3 & \omega_2 \\ \omega_3 & 0 & -\omega_1 \\ -\omega_2 & \omega_1 & 0 \end{pmatrix}, \quad (8)$$

we can obtain the position and the orientation of each filament. This method is simple to implement and singularity-free.

## 2 How to Obtain the Stiffness of Tail Domain Binding

Another key issue in our modeling effort is how to treat tail domain binding. As mentioned in the main text, we opted to treat the tail domain binding as a spring connection. The binding potential energy is written as

$$U = \frac{1}{2}k (\|\mathbf{p}_i - \mathbf{p}_j\| - d_0)^2 \quad (9)$$

where  $\mathbf{p}_i = \mathbf{r}_i + R_i \mathbf{a}_i$  denotes the binding point, where the subscript  $i$  refers to the filament on which this point is described. See Figure 1 below for a graphical explanation. That is, we only consider a linear spring connection.  $d_0$  denotes the intrinsic, or energetically favorable, distance between the center lines of two filaments.

The value of  $k$  is not currently known. One way to estimate it is to relate it to the free energy  $\Delta G$ . Mathematically speaking, we expand the binding free energy  $F$  around the reference or intrinsic points:  $F = F_0 + \left. \frac{\partial F}{\partial \mathbf{x}} \right|_{\mathbf{x}_0} (\mathbf{x} - \mathbf{x}_0) + \frac{1}{2} (\mathbf{x} - \mathbf{x}_0)^T \left. \frac{\partial^2 F}{\partial \mathbf{x}^2} \right|_{\mathbf{x}_0} (\mathbf{x} - \mathbf{x}_0)$ . Here  $\mathbf{x}$  and  $\mathbf{x}_0$  denote the configuration variable and its intrinsic value. Since  $\left. \frac{\partial F}{\partial \mathbf{x}} \right|_{\mathbf{x}_0} = \mathbf{0}$ , we only have two terms to consider.  $F_0$  is a constant term which is equal to  $\Delta G$ , and the last term which is written as the sum of quadratic terms without coupling becomes  $U$ . Applying this into our current model, the energy is written as

$$F = \Delta G + \frac{1}{2}k (\|\mathbf{p}_i - \mathbf{p}_j\| - d_0)^2. \quad (10)$$

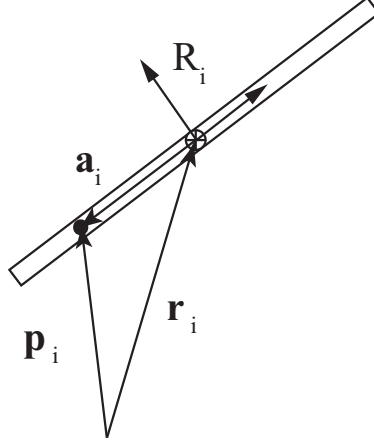


Figure 1: Schematic illustration of filament configuration

The spring constant  $k$  can be calculated from the position where  $F = 0$  at  $d = d_{\text{cutoff}}$ . In other words,

$$k = \frac{-2\Delta G}{(d_{\text{cutoff}} - d_0)^2} \quad (11)$$

where  $d_{\text{cutoff}} = \|\mathbf{p}_i - \mathbf{p}_j\|_{F=0}$ . From this, we can estimate the stiffness  $k$ .

Now let us discuss how to obtain  $\Delta G$ . Since we know that  $K_d = 2 \mu\text{M}$  for the interaction between K14's tail domain and K5-K14 filaments, we can determine the free energy change for a tail domain binding in the standard state (i.e., 1 M concentration of filaments, tail domains and tail-filament complexes) by using (3):

$$K_d = \exp\left(\frac{\Delta G^0}{k_B T}\right). \quad (12)$$

In other words,

$$\Delta G^0 = k_B T \ln(K_d). \quad (13)$$

Numeric value of the standard free energy is  $\Delta G^0 = -0.054 \text{ [pN}\cdot\mu\text{m}] = -54 \text{ [pN}\cdot\text{nm}]$ . Then the free energy in our situation is computed as (3)

$$\Delta G = \Delta G^0 - k_B T \ln\left(\frac{[T]_c [F]_c}{[TF]_c}\right) \quad (14)$$

where  $[T]_c = 1 \text{ mg/mL} = 18.18 \mu\text{M}$  in this case. T and F denotes the tail domain and keratin filament, respectively. Looking at figure 2B' in (4), one can see that at the concentration above  $15 \mu\text{M}$ , the bound fraction is 1, which means  $[TF]_c \approx [F]_c$ . In case when  $[T]_c = 18.18 \mu\text{M}$ ,  $\Delta G = -0.0091 \text{ [pN}\cdot\mu\text{m}]$ . This represents the free energy for one tail domain binding event in the current work.

The spring constant of a binding event can then be calculated from the consideration of  $\Delta G$  with  $d_{\text{cutoff}} = 15 \text{ nm}$  as  $k = 726.5 \text{ pN}/\mu\text{m}$ . Note that the stiffness of a single myosin head attached to actin is measured as  $1.2 \text{ pN/nm}$  (5). Hence our estimation of binding stiffness appears to be within a reasonable range. Importantly, once a tail domain and its binding site bind together, then they are treated as connected by a spring of which the stiffness is  $k$ , as detailed above. This association

event is described with the cut-off distance. Detachments are described with a single parameter, dissociation rate constant, as conveyed in the main text.

### 3 Details on the Dissociation Rate Constant

We first would like to calculate the possible range of association/dissociation rate constants from the experiments reported in (4). We start from the fact that  $K_d = 2 \mu\text{M}$  for K14 tail binding domain in order to determine the dissociation rate constant  $k_{\text{off}}$ . Given that K14's tail domain is 52 amino acid residues in length, one can estimate its size as a particle to be about  $0.8 \sim 5 \text{ nm}$ , whether it is treated as a freely jointed chain entangled in the solution, or fully stretched. The association rate constant  $k_{\text{on}}$  in this case then can be computed as (6–8):

$$k_{\text{on}} = 4\pi D_0 d_c \quad (15)$$

where  $d_c$  denotes the effective distance within which a given tail particle and its binding site are considered bound. The diffusion coefficient of the particle is denoted as  $D_0$ . Since we elected a  $\sim 5 \text{ nm}$  effective distance  $d_c$  between the free tail particle and the binding site on the filament, we obtain  $k_{\text{on}} = 1.6 \sim 10 \mu\text{M}^{-1}\text{s}^{-1}$ . Therefore we choose the association rate constant to be  $5 \mu\text{M}^{-1}\text{s}^{-1}$ , with the associated dissociation rate constant being  $10 \text{ s}^{-1}$ . This is consistent with the assumption that  $d_{\text{cutoff}} = 15 \text{ nm}$ , as conveyed in the main text.

## 4 Computational Details

### 4.1 Tail Binding

In this section, we explain how to actually implement the Langevin equation. As mentioned, we treat this binding as a spring-like connection. Let us detail this notion with a single point contact binding event (see Figure 2 below). Let  $g_i = (\mathbf{r}_i, R_i)$  and  $g_j = (\mathbf{r}_j, R_j)$  denote the position and orientation of the center of mass of the  $i$ -th and the  $j$ -th filament, respectively. The location of a contact/binding point from the center of mass of each filament is denoted  $\mathbf{a}_i$  and  $\mathbf{a}_j$ . These position vectors are viewed from the body-fixed frames.  $\mathbf{a}_i^s$  denotes the same vector viewed from the spatial frame of reference.

The force acting on the  $i$ -th rod by the  $j$ -th rod is computed by the aforementioned potential energy as

$$\mathbf{f}_{ij}^s = -\frac{\partial U}{\partial \mathbf{p}_i} = -k (\|\mathbf{p}_i - \mathbf{p}_j\| - d_0) \frac{\mathbf{p}_i - \mathbf{p}_j}{\|\mathbf{p}_i - \mathbf{p}_j\|}. \quad (16)$$

Since the point of force has a different location than the center of mass, it exerts a moment as well. In total, the wrench acting on the  $i$ -th rod which is viewed from the spatial frame is computed as

$$\mathbf{F}_i^s = \begin{pmatrix} \boldsymbol{\tau}_{ij}^s \\ \mathbf{f}_{ij}^s \end{pmatrix} = \begin{pmatrix} \mathbf{a}_i^s \times \mathbf{f}_{ij}^s \\ \mathbf{f}_{ij}^s \end{pmatrix}. \quad (17)$$

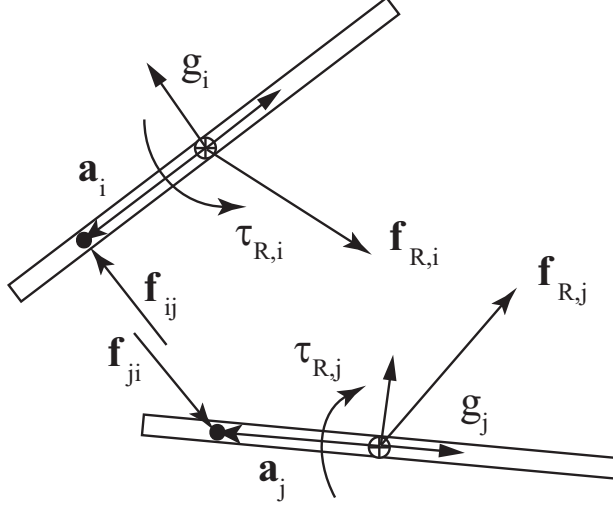


Figure 2: Schematic cartoon explaining the equation of motion for the spring-like binding event

Changing view from the spatial frame to body frame can be done as

$$\mathbf{F}_i = \mathcal{R}_i^T \mathbf{F}_i^s \quad (18)$$

where

$$\mathcal{R}_i = \begin{pmatrix} R_i & 0_{3 \times 3} \\ 0_{3 \times 3} & R_i \end{pmatrix} \quad (19)$$

In the case of contact through many points, we still can use the aforementioned approach although genesis of corresponding pairs of contact becomes an important consideration. Since we treat each filament as a rigid rod with pre-fixed tail and binding domains on it, we can calculate the distance and corresponding points on both participating filaments (or lines). We pick the nearest tail or binding domain site relative to the point from which the distance is calculated. Then we can select pairs of sites until the distance between those paired sites are within the cut-off distance specified. Wrenches can then be summed up. In this manner, we can compute the total wrench (moment and force) applied on the filament more efficiently.

The actual integration of the differential equations is as follows. First, we compute the velocity using the Langevin equation for each filament as

$$\Gamma \dot{\boldsymbol{\xi}}(t) = \mathbf{F}(t) + \mathbf{F}_R(t). \quad (20)$$

Then the position and orientation of each filament is updated as

$$g(t) = g(t - \Delta t) \exp \left[ \Delta t \widehat{\boldsymbol{\xi}}(t) \right], \quad (21)$$

or one can use the trapezoidal method as

$$g(t) = g(t - \Delta t) \exp \left[ \frac{\Delta t}{2} \left( \widehat{\boldsymbol{\xi}}(t) + \widehat{\boldsymbol{\xi}}(t - \Delta t) \right) \right]. \quad (22)$$

Time step in dynamic simulation is important. It is known that for a particle connected by a spring whose stiffness is  $k$ , time constant is  $\tau = \gamma/k$  (3). Time scale smaller than this is considered correlated motion, whereas larger time scale renders uncorrelated motion. Due to the nature of a rod having different drag coefficients, this time constant varies from  $10^{-10}$  sec to  $10^{-6}$  sec in our study. One also has to consider the effect of time step on the spring force. When two filaments become sufficiently close each other, a stiff spring is bound to generate unnaturally large force given small displacement between filaments, if the time step is not sufficiently small. On the other hand, a higher computation cost is generated when the time step value is made too small. In our study, we first calculate  $\tau = \min(\Gamma/k)$ . After considering all these elements, we choose  $\Delta t = \tau \times 10 \sim \tau \times 100$  seconds.

## 4.2 Filament Interactions

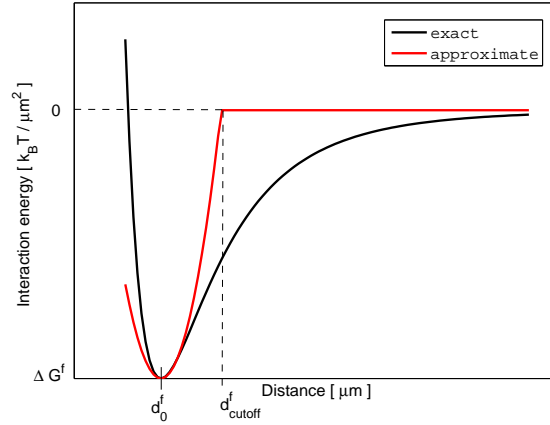


Figure 3: Possible energy form of filament interaction and its approximate version used in the study. Any type of interactions with both attractive and repulsive parts can be approximated with this function. The main parameters are  $\Delta G^f$ ,  $d_{\text{cutoff}}^f$ , and  $d_0^f$  which are functions of ionic strength in the solution.

As stated in the main text, we use the following simple form of energy

$$U^f = \Delta G^f + \frac{1}{2}k^f (d^f - d_0^f)^2. \quad (23)$$

where  $\mathbf{p}_i = \mathbf{r}_i + R_i[\ell_i \ 0 \ 0]^T$  and  $d^f = \|\mathbf{p}_i - \mathbf{p}_j\|$ . Figure 3 provides a graphical account of the approximate energy and its parameters, which are function of the ionic strength in the solution. Then the force between infinitesimal segments on each filament is computed as

$$\delta \mathbf{f}_{ij}^s = -k^f (d^f - d_0^f) \frac{\mathbf{p}_i - \mathbf{p}_j}{d^f} \quad (24)$$

and  $\delta \mathbf{f}_{ji}^s = -\delta \mathbf{f}_{ij}^s$ . Then we can apply a force as

$$\mathbf{f}_{ij}^s = \int_{\ell_1=-L/2}^{L/2} \int_{\ell_2=-L/2}^{L/2} \delta \mathbf{f}_{ij}^s d\ell_2 d\ell_1. \quad (25)$$



Moments are

$$\mathbf{m}_{ij}^s = \int_{\ell_1} \int_{\ell_2} \ell_1 R_i \mathbf{e}_1 \times \delta \mathbf{f}_{ij}^s d\ell_2 d\ell_1 \quad (26)$$

and

$$\mathbf{m}_{ji}^s = \int_{\ell_1} \int_{\ell_2} \ell_2 R_j \mathbf{e}_1 \times \delta \mathbf{f}_{ji}^s d\ell_2 d\ell_1. \quad (27)$$

Explicitly,

$$\mathbf{f}_{ij}^s = \int_{\ell_1=-L/2}^{L/2} \int_{\ell_2=-L/2}^{L/2} \left[ -k^f (\mathbf{r}_i - \mathbf{r}_j) + k^f d_0^f (\mathbf{r}_i - \mathbf{r}_j) \frac{1}{d^f} + k^f d_0^f R_i \mathbf{e}_1 \frac{\ell_1}{d^f} - k^f d_0^f R_j \mathbf{e}_1 \frac{\ell_2}{d^f} \right] d\ell_2 d\ell_1, \quad (28)$$

$$\mathbf{m}_{ij}^s = \int_{\ell_1} \int_{\ell_2} \left[ R_i \mathbf{e}_1 \times k^f d_0^f (\mathbf{r}_i - \mathbf{r}_j) \frac{\ell_1}{d^f} + R_i \mathbf{e}_1 \times \left( -k^f d_0^f R_j \mathbf{e}_1 \right) \frac{\ell_1 \ell_2}{d^f} \right] d\ell_2 d\ell_1 \quad (29)$$

and

$$\mathbf{m}_{ji}^s = \int_{\ell_1} \int_{\ell_2} \left[ -R_j \mathbf{e}_1 \times k^f d_0^f (\mathbf{r}_i - \mathbf{r}_j) \frac{\ell_2}{d^f} - R_j \mathbf{e}_1 \times \left( k^f d_0^f R_i \mathbf{e}_1 \right) \frac{\ell_1 \ell_2}{d^f} \right] d\ell_2 d\ell_1. \quad (30)$$

In order to obtain these forces and moments, we perform numerical integrations. It is worth noting that the unit of the interaction energy is  $k_B T / \mu m^2$ , not  $k_B T$ . This therefore affects the unit of  $k$ . This approach is mathematically exact in calculating interaction forces. Once we compute the force and the torque, the algorithm already explained in the previous section is applied.

Another important issue to consider is the periodic boundary condition. Balancing the number of filaments which cross the boundaries is insufficient because of filament interactions. In order to truly reflect the continuum characteristics of the simulation space, we copy the rectangular parallelepiped part of which the thickness corresponds to half the length of a filament from each side of the cubic space and paste it onto the opposite side. This is done at every time step during the simulation. In this manner one can take the effect of having filaments outside the cubic space into account.

## References

1. Chirikjian, G. S., and A. B. Kyatkin, 2001. Engineering Applications of Noncommutative Harmonic Analysis. CRC Press.
2. Kim, J. S., 2006. A group theoretic and statistical mechanical treatment of chainlike structures. Ph.D. thesis, the Johns Hopkins University.
3. Howard, J., 2001. Mechanics of Motor Proteins and the Cytoskeleton. Sinauer Associates, Inc.
4. Bousquet, O., L. Ma, S. Yamada, C. Gu, T. Idei, K. Takahashi, D. Wirtz, and P. A. Coulombe, 2001. The nonhelical tail domain of keratin 14 promotes filament bundling and enhances the mechanical properties of keratin intermediate filaments in vitro. *Journal of Cell Biology* 155:747–753.
5. Linari, M., M. Caremani, C. Piperio, P. Brandt, and V. Lombardi, 2007. Stiffness and fraction of myosin motors responsible for active force in permeabilized muscle fibers from rabbit psoas. *Biophys. J.* 92:2476–2490.

6. Berg, O. G., 1984. Diffusion-controlled protein-DNA association: Influence of segmental diffusion of the DNA. *Biopolymers* 23:1869–1889.
7. Northrup, S. H., and J. T. Hynes, 1979. Short range caging effects for reactions in solution. I. Reaction rate constants and short range caging picture. *Journal of Chemical Physics* 71:871–883.
8. Northrup, S. H., S. A. Allison, and J. A. McCammon, 1984. Brownian dynamics simulation of diffusion-influenced bimolecular reactions. *Journal of Chemical Physics* 80:1517–1524.

# Modeling the Self-Organization Property of Keratin Intermediate Filaments: Supporting Data

Jin Seob Kim<sup>1</sup>, Chang-Hun Lee<sup>1</sup>, and Pierre A. Coulombe<sup>1,2,3</sup>

<sup>1</sup>Dept. of Biochemistry and Molecular Biology, Bloomberg School of Public Health, the Johns Hopkins University, Baltimore, MD 21205, USA  
Dept. of <sup>2</sup>Biological Chemistry, and <sup>3</sup>Dermatology, School of Medicine, the Johns Hopkins University, Baltimore, MD 21205, USA

## Contents:

- Supplemental Figure Legends
- Supplemental Figures
  1. Figure S1: Simulation results without tail domain binding events
  2. Figure S2: Simulation results with tail domains as free particles
- Supplemental Movies
  1. Movie S1: Filament network topology achieved when only tail domain binding events are included (see Fig. 1B in main text).
  2. Movie S2: Filament network topology achieved when tail domain binding events and long-range interactions between filaments are included (see Fig. 2B in main text).
  3. Movie S3: Filament network topology achieved when tail domain binding events are reversible ( $k_{\text{on}} = 5 \mu\text{M}^{-1}\text{s}^{-1}$ ;  $k_{\text{off}} = 10 \text{s}^{-1}$ ) (see Fig. 3A in main text).
  4. Movie S4: Filament network topology achieved when filaments are longer ( $L = 2 \mu\text{m}$ ) (see Fig. 3B in main text).
  5. Movie S5: Filament network topology achieved when filaments are shorter ( $L = 0.5 \mu\text{m}$ ) (see Fig. 4C in main text).

## Supplemental Figure Legends

**Fig. S1:** Simulation results of filament behavior in the presence of long-range filament interactions, minus the contribution of tail domain-mediated binding events, after  $5 \times 10^5$  steps (equivalently, after 21.6 ms). The parameters defining long-range interactions are:  $\Delta G^f = -100 k_B T / \mu m^2$ ,  $d_0^f = 20$  nm, and  $d_{\text{cutoff}}^f = 40$  nm. (A) Final configuration; (B) Filament RMSD. Note that self-avoiding effects between filaments are not included in the simulation; including them would lead to a configuration similar to that reported in (1).

**Fig. S2:** Simulation results when tail domains exist as free particles, as opposed to covalently bound on polymerized K14 molecules. The numbers of filaments and tail domain copies are the same as in the previous simulations (Fig. 1 and 2). Time step was chosen as  $t \sim 4.3$  ns. The cut-off distance for the tail particle binding is now 7.5 nm which is the half of that prevailing in the previous simulation (Fig. 1 and 2); this makes it consistent with previous simulations in which the cut-off distance is 15 nm. One particle is allowed to bind to a maximum of two filaments. In this simulation, we included dissociation effect for tail particles (see Fig. 3 in the main text). (A) Initial Configuration; (B) Configuration after 0.74 ms ( $n = 2 \times 10^5$  steps) with inclusion of filament interactions and tail binding events; (C) Configuration after 2.6 ms ( $n = 6 \times 10^5$  steps) with tail binding events but without long-range interactions between filaments; (D) Number of particles making a bridged connection between two filaments as outlined in case (B); (E) Number of particles making a bridged connection between two filaments as outlined in case (C); (F) Number of particles bound to filaments, or number of pairs, as outlined in case (B); (G) Number of pairs as outlined in case (C). These results show that there is a huge disadvantage in the crosslinked network formation when the tail domains exist as free particles. This conclusion partly explains why keratins have evolved into the current form, i.e., with filament binding sites present *in cis* on keratin proteins.

## Reference for the Legends

Cui, H., E.T. Pashuck, Y.S. Velichko, S.J. Weigand, A.G. Cheetham, C.J. Newcomb, and S.I. Stupp, 2010. Spontaneous and X-ray-triggered crystallization at long range in self-assembling filament networks. *Science* 327: 555–559.

# Supplemental Figures

Fig. S1

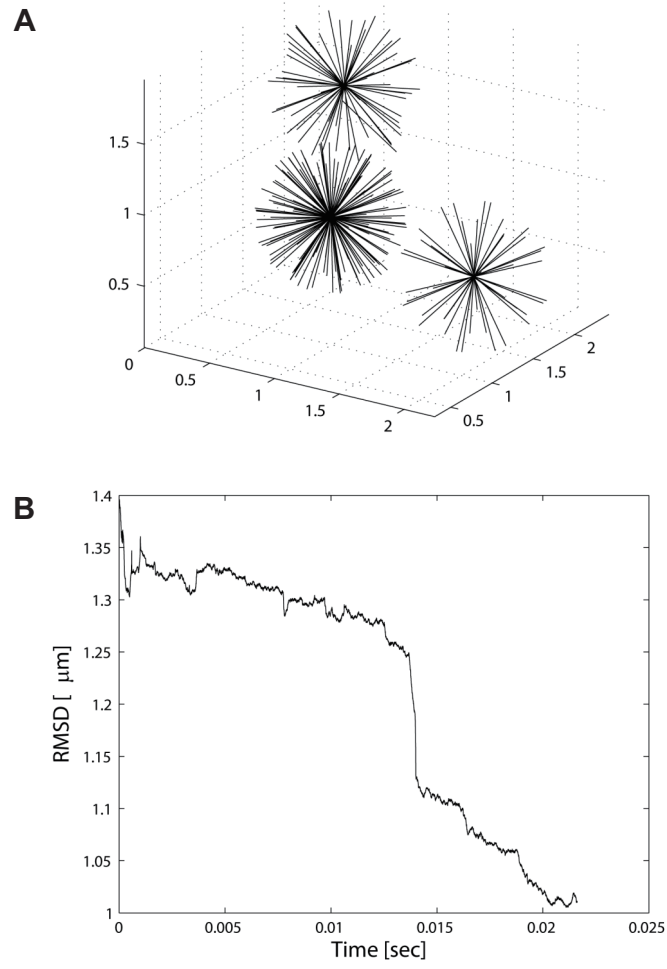
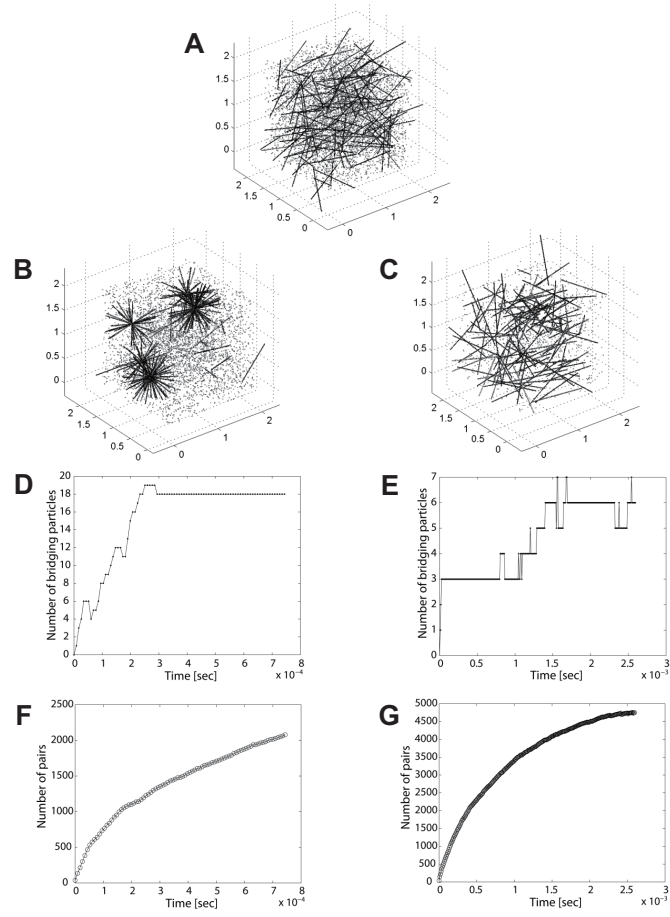


Fig. S2



## Supplemental Movies

- **Movie S1:** Time evolution of configuration shown in Fig. 1*B* in the main text. Filament network topology achieved when only tail domain binding events are included.
- **Movie S2:** Time evolution of configuration shown in Fig. 2*B* in the main text. Filament network topology achieved when tail domain binding events and long-range interactions between filaments are included.
- **Movie S3:** Time evolution of configuration shown in Fig. 3*A* in the main text. Filament network topology achieved when tail domain binding events are reversible ( $k_{\text{on}} = 5 \mu\text{M}^{-1}\text{s}^{-1}$ ;  $k_{\text{off}} = 10 \text{s}^{-1}$ ).
- **Movie S4:** Time evolution of configuration shown in Fig. 3*B* in the main text. Filament network topology achieved when filaments are longer ( $L = 2 \mu\text{m}$ ).
- **Movie S5:** Time evolution of configuration shown in Fig. 4*C* in the main text. Filament network topology achieved when filaments are shorter ( $L = 0.5 \mu\text{m}$ ).